

OPEN

Silver vacancy concentration engineering leading to the ultralow lattice thermal conductivity and improved thermoelectric performance of $\text{Ag}_{1-x}\text{InTe}_2$

Yaqiong Zhong^{1,2}, Yong Luo^{1*}, Xie Li² & Jiaolin Cui^{2*}

AgInTe_2 compound has not received enough recognition in thermoelectrics, possibly due to the fact that the presence of Te vacancy (V_{Te}) and antisite defect of In at Ag site (In_{Ag}) degrades its electrical conductivity. In this work, we prepared the $\text{Ag}_{1-x}\text{InTe}_2$ compounds with substoichiometric amounts of Ag and observed an ultralow lattice thermal conductivity ($\kappa_{\text{L}} = 0.1 \text{ W m}^{-1} \text{ K}^{-1}$) for the sample at $x = 0.15$ and 814 K. This leads to more than 2-fold enhancement in the ZT value ($ZT = 0.62$) compared to the pristine AgInTe_2 . In addition, we have traced the origin of the ultralow κ_{L} using the Callaway model. The results attained in this work suggest that the engineering of the silver vacancy (V_{Ag}) concentration is still an effective way to manipulate the thermoelectric performance of AgInTe_2 , realized by the increased point defects and modified crystal structure distortion as the V_{Ag} concentration increases.

Thermoelectrics (TE) materials can transfer energy from heat to electricity or vice versa due to their inherent Seebeck or Peltier effects. However, the TE device at present is still inefficient up to date mainly due to low TE performance or ZT value of the materials, which is defined as $ZT = \alpha^2 \sigma T / \kappa$, where α , σ , T , and κ are each the Seebeck coefficient, electrical conductivity, absolute temperature, and total thermal conductivity consisting of electronic (κ_{e}) and lattice (κ_{L}) components. Therefore, it is quite necessary to explore novel TE candidates. Ternary I-III-VI₂ (I = Cu, Ag; III = Al, Ga, In; VI = S, Se, Te) chalcogenides, such as CuGaTe_2 ¹, CuInTe_2 ², AgInSe_2 ³ and AgGaTe_2 ^{4,5}, have recently attracted much attention in thermoelectrics because of their unique crystal and band structures^{6,7}, among which the cation vacancy and crystal structure are two important factors in engineering both the carrier concentration and phonon transport^{8–10}. However, to our best knowledge, AgInTe_2 has not received due recognition. The possible reason is the presence of the defects V_{Te} and In_{Ag} in AgInTe_2 , which were identified through analyzing the electrical data of AgInTe_2 by Bellabarba etc¹¹. These two defects, which are vital to the formation of two shallow donor levels at around 9 mV and 28 mV below the conduction band minimum (CBM)¹¹, directly degrade the electrical conductivity ($10^3 \sim 10^6 \text{ m}\Omega\text{cm}$ at 300–700 K)^{12,13}. As a consequence, the highest ZT value of AgInTe_2 is only 0.07 at 600 K¹³. The temperature at which the highest ZT value was attained is just about half the melting point of AgInTe_2 (see the phase diagram in Fig. S1). In this regard, it is important to eliminate the defects V_{Te} and/or In_{Ag} in order to improve the TE performance of AgInTe_2 .

On the other hand, the Debye temperature (Θ_{D}) and average sound velocity of AgInTe_2 are 113–202 K and $\nu_{\text{age}} = 1240 \text{ ms}^{-1}$ respectively^{11,14,15}, which are very low compared to those of CuInTe_2 ($\Theta_{\text{D}} = 197.5 \text{ K}$; $\nu_{\text{age}} = 3420 \text{ ms}^{-1}$)¹⁶ and CuGaTe_2 ($\Theta_{\text{D}} = 229.0 \text{ K}$; $\nu_{\text{s}} = 2072.0 \text{ ms}^{-1}$, $\nu_{\text{l}} = 3817.0 \text{ ms}^{-1}$)¹. Besides that, the average sound velocity is only about half that of AgGaTe_2 ($\nu_{\text{s}} = 1812.0 \text{ ms}^{-1}$, $\nu_{\text{l}} = 2990.0 \text{ ms}^{-1}$)⁷. It implies that the compound AgInTe_2 , naturally, has a low lattice thermal conductivity¹⁷, hence it is potentially a good TE candidate. Apart from that, AgInTe_2 has a relatively less silver vacancy formation enthalpy ($\Delta H_{\text{V}}(\text{Ag}) = 2.90 \text{ eV}$) than most ternary I-III-VI₂ chalcogenides, except for CuInTe_2 ($\Delta H_{\text{V}}(\text{Cu}) = 2.59 \text{ eV}$) and CuGaTe_2 ($\Delta H_{\text{V}}(\text{Cu}) = 2.73 \text{ eV}$)¹⁸. Therefore, from the thermodynamics point of view, AgInTe_2 with substoichiometric amounts of Ag should be more stable than most of them. The presence of substoichiometric Ag eliminates the V_{Te} and forms the silver

¹School of Materials Science and Engineering, China University of Mining and Technology, Xuzhou, 221116, China.

²School of Materials and Chemical Engineering, Ningbo University of Technology, Ningbo, 315211, China. *email: sulyflying@cumt.edu.cn; cuijiaolin@163.com

vacancy V_{Ag} and thereby might increase the point defect scattering of phonons while improving the electrical conductivity simultaneously⁵.

Motivated by the above priorities of AgInTe₂ with substoichiometric amounts of Ag in thermoelectrics, we believe that there is still some room to improve its TE performance. Therefore, in this work we prepared Ag_{1-x}InTe₂ (here the x value representing the Ag deficiency, and the Ag vacancy concentration (V_{Ag}), $V_{\text{Ag}} = x/2$) and then examined their TE performance in the range from room temperature (~RT) to ~820 K.

Experimental Procedures

Syntheses and preparation of samples. The three elements Ag, In and Te, were loaded into different vacuum silica tubes, according to the chemical compositions of Ag_{1-x}InTe₂ ($x = 0, 0.05, 0.1, 0.15$ and 0.2). They were then heated to 1073 K in 30 min and held at this temperature for 48 h. After that, the ingots were cooled down to 873 K in 8 h before being quenched in water. Subsequently, they were annealed at 553 K for 72 h. After cooling to RT, the ingots were ball milled for 5 h, and the dried powders were then rapidly sintered using the spark plasma sintering apparatus (SPS-1030) specifically programmed with a peak temperature of 823 K and pressure of 55 MPa. The densities of the sintered bulks were measured by using the Archimedes' method. The bulk samples about the size of $2.5 \times 3 \times 12 \text{ mm}^3$ were prepared for electrical property measurements, and those of $\phi 10 \times 1.5 \text{ mm}^2$ for thermal diffusivity measurement.

Analyses and measurements. The Hall coefficient (R_{H}) at RT were measured by using a PPMS (Model-9) with a magnetic field sweeping between $\pm 5.0 \text{ T}$. The Hall mobility (μ) and carrier concentration (n_{H}) were subsequently determined based on the equations $\mu = |R_{\text{H}}|\sigma$ and $n_{\text{H}} = 1/(eR_{\text{H}})$, respectively (e is the electron charge).

The Seebeck coefficients and electrical conductivities were evaluated by using ZEM-3 under a helium atmosphere at a temperature ranging from ~RT to ~820 K, with an uncertainty of <5.0% for each. The thermal diffusivities were measured by using TC-1200RH, with an uncertainty of <10.0%. The heat capacities (C_{p}) of the present materials were estimated by using the Dulong-Petit rule, $C_{\text{p}} = 3nR$ (here n is the number of atoms per formula unit and R is the gas constant). The C_{p} estimation is used in AgInTe₂ or its related systems by many works^{13,19,20}, and is proved to be in a good agreement with (or only ~6% higher than) the measured one^{13,20}, as the C_{p} values above Debye temperature (Θ_{D}) are almost unchanged²¹. When calculating the electronic thermal conductivities (κ_{e}) according to the equation $\kappa_{\text{e}} = L\sigma T$, the Lorenz numbers L were estimated by using the formula $L = 1.5 + \exp(-|\alpha|/116)$ ²², (where L is in $10^{-8} \text{ W } \Omega \text{ K}^{-2}$ and α in $\mu\text{V K}^{-1}$). The total uncertainty for ZT was ~20%.

Analyses. The chemical compositions were determined by using an electron probe micro-analyzer (EPMA) (S-4800, Hitachi, Japan) with an accuracy of >97%.

The powder X-ray diffraction patterns of the samples were registered by using X-ray powder diffractometer (XRD) (D8 Advance) operating at 50 kV and 40 mA in a step size of 0.02° in the range of 10° to 100° , and a X'Pert Pro, PANalytical code was used to do the Rietveld refinement of the XRD patterns with a step size of 0.01° using the same operating voltage and current. The lattice constants a and c were directly obtained from the refinement of the X-ray data using the Jade software.

Differential scanning calorimeter (DSC) is conducted in a Netzch STA 449 F3 Jupiter equipped with a TASC414/4 controller. The instrument is calibrated from a standard list. The sample of the powder ($x = 0.15$) is loaded into an open alumina crucible. The measurement is performed between ~300 K to ~820 K with a heating rate of 5 K min^{-1} in Ar atmosphere.

Results and Discussion

Chemical compositions and X-ray diffraction patterns. The scanning electron microscopy (SEM) images of both polished and freshly fractured surface, three mappings of elements (Ag, In, Te) as well as the energy-dispersive x-ray spectroscopy (EDS) of the sample at $x = 0.15$ are shown in Fig. S2a–f. The analyzed chemical compositions of substoichiometric Ag_{1-x}InTe₂ ($x = 0.15$) are shown in Table S1, where the number of Te moles is normalized to 2.0. From the analyzed results, it is observed that there is a slight Te evaporation during the sample preparation process. Further, the element distribution is not uniform in the matrix, mainly due to the precipitation of the second phases. Also, the densities of the sintered bulks Ag_{1-x}InTe₂ ($x = 0\text{--}0.2$), ranging from $5.92 \times 10^3 \text{ kg/m}^3$ ($x = 0$) to $5.97 \times 10^3 \text{ kg/m}^3$ ($x = 0.2$), are about ~96.0% of the theoretical one ($6.17 \times 10^3 \text{ kg/m}^3$) of AgInTe₂. The low density of the materials is detrimental to the electrical conductivity, even though it is helpful to scatter phonons.

The refinements of the powder X-ray diffraction (XRD) patterns of the four Ag_{1-x}InTe₂ samples ($x = 0, 0.1, 0.15, 0.2$) are shown in Fig. S3. The results involving the crystallographic data, Wyckoff positions, atomic coordinates and site occupancy factors (SOFs) are listed in Table S2–5, where the SOFs of Ag (4a), In (4b) and Te (8d) are all 1.0 in AgInTe₂ without the antisite defect In_{Ag} identified. In addition, the main peaks of the patterns are indexed to the existing chalcopyrite AgInTe₂ (PDF: 65–0355) with the minor impurities AgTe₃ (1.3 wt.% at $x = 0$) and Te (less than 3.1 wt.% at $x = 0, 0.15, 0.2$) precipitated. In order to prevent the precipitation of the impurities AgTe₃ and Te from the main phase AgInTe₂, all the samples were subject to heat treatment at 813 K for 72 h. After the heat treatment, the materials were purified without any impurity phases in the samples at $x = 0\text{--}0.1$, and only trace Te element still exists in the samples at $x = 0.15$ and 0.2 , as shown in the refined XRD patterns in Fig. S4. The crystallographic data, Wyckoff positions, atomic coordinates and site occupancy factors (SOFs) in the heat-treated samples are not shown here.

Figure 1a presents the lattice constants as a function of x value for the Ag_{1-x}InTe₂ samples with or without heat treatment, where it is observed that the lattice constants a and c of two set samples decrease almost linearly, following the Vegard's law. This is indicative of the shrinkage of the crystal structure. Apart from that, the tetragonal distortion parameter η value ($\eta = c/2a$) of non-heat treated samples increases from 0.9825 ($x = 0$) to 0.9853

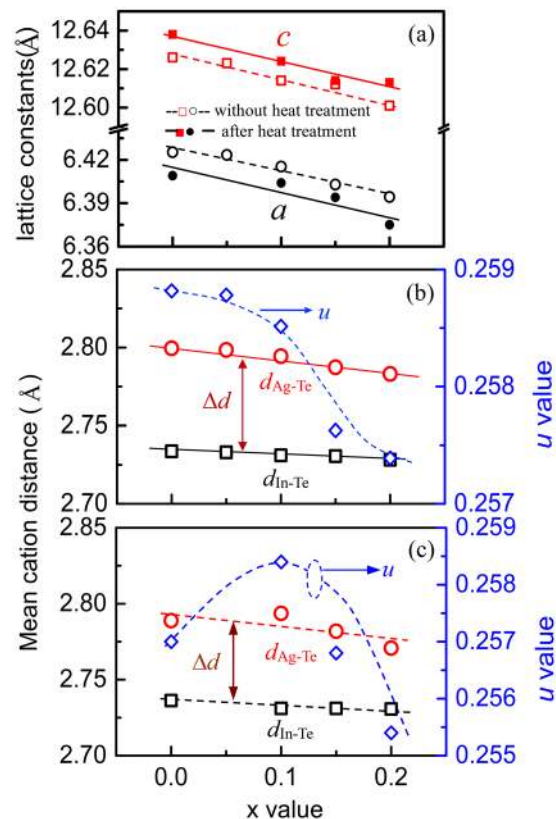


Figure 1. (a) Lattice constants a and c as a function of x value in $\text{Ag}_{1-x}\text{InTe}_2$ for the samples with or without heat treatment. (b,c) Structural parameters involving cation (anion)-Te distances ($d_{\text{Ag-Te}}$, $d_{\text{In-Te}}$) and anion position displacement parameter (u) as a function of x value in $\text{Ag}_{1-x}\text{InTe}_2$. (b) For the samples without heat treatment; (c) For the samples with heat treated at 813 K for 72 h.

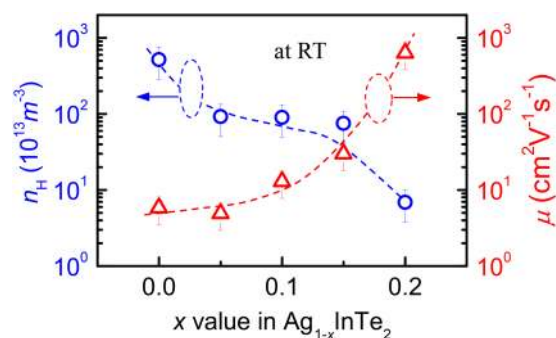


Figure 2. Hall carrier concentration (n_{H}) and mobility (μ) at RT as a function of x value in $\text{Ag}_{1-x}\text{InTe}_2$ without heat treatment.

($x=0.2$) (see Tables S2, 6) and the anion position displacement parameter u decreases from 0.2588 ($x=0$) to 0.2573 ($x=0.2$) as the x value increases. The u value of AgInTe_2 is less than the reported value of 0.2618²³. Besides, the difference (Δd) between the cation and anion distances ($\Delta d = d_{\text{Ag-Te}} - d_{\text{In-Te}}$) tends to be small (see Fig. 1b). A similar tendency was also observed in the heat-treated samples, as shown in Fig. 1c and Table S6, where the u value starts to decrease above $x=0.1$. These results suggest that the crystal structure distortion of $\text{Ag}_{1-x}\text{InTe}_2$ exists ($u > 0.25$) but tends to be weakened as the cation Ag vacancy concentration increases, in spite of the presence of a minor impurity Te.

Transport properties and TE performance. In order to gain a better understanding of the effect of the crystal structure and Ag vacancy engineering on the transport properties, we have measured the Hall coefficients (R_{H}) at RT for non-heat treated samples, and then calculated the Hall carrier concentrations (n_{H}) and mobility (μ). The results are shown in Fig. 2, in which the n_{H} value generally decreases from $5.19 \times 10^{16} \text{ cm}^{-3}$ to $6.9 \times 10^{14} \text{ cm}^{-3}$ as the x value (or V_{Ag}) increases, and that the μ value increases from $5.83 \text{ cm}^2/\text{Vs}$ to $636.7 \text{ cm}^2/\text{Vs}$. This indicates

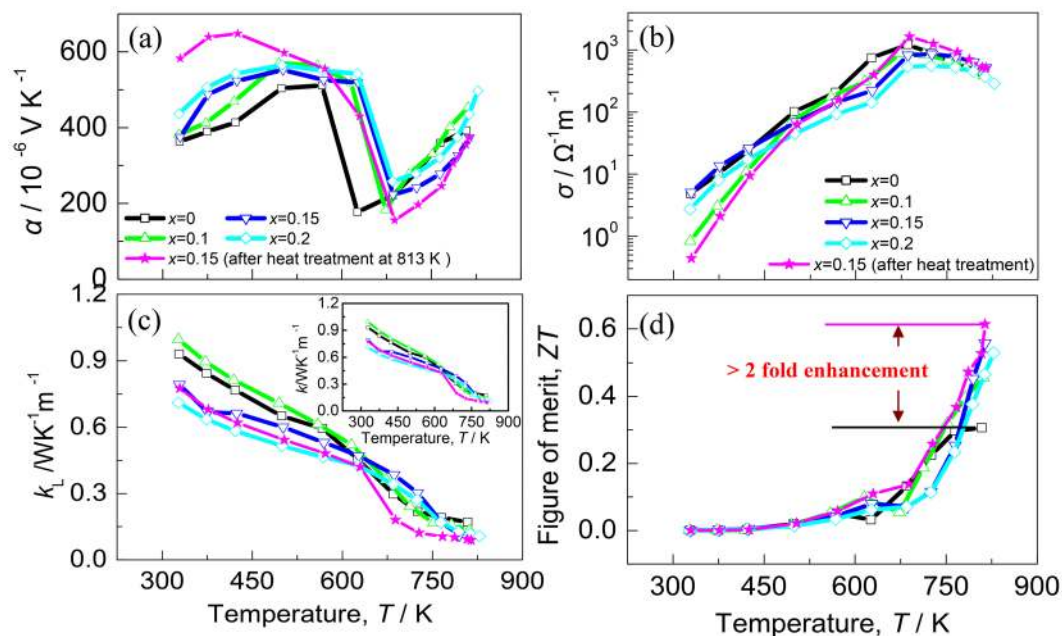


Figure 3. Thermoelectric performance of $\text{Ag}_{1-x}\text{InTe}_2$ without heat treatment as a function of temperature for different x values. (a) Seebeck coefficients (α) with different x values; (b) Electrical conductivities (σ) with different x values; (c) Lattice thermal conductivities (κ_L) with different x values, an inset is the total thermal conductivities (κ); (d) ZT values as a function of temperature. Besides that, the TE performance of the sample at $x=0.15$ after heat treatment at 813 K for 72 h was presented for comparison.

that Ag cation vacancy has a negative effect on the carrier concentration. Such an effect, which has been reported in many materials, such as Cu-Ga(In)-Te ternary compounds^{24–26}, can be elucidated by unpinning the Fermi level (E_F) followed by its movement towards the conduction band (CB)^{27,28}. As a consequence, the p-type holes is neutralized and the carrier concentration is thus reduced. Although the R_H values might be affected by the presence of the Te and/or AgTe_3 , it is believed that the impact should be minimum, due to the limited contents of the impurities. Plus, the n_H value is rather low compared to the reported counterparts CuInTe_2 ($>1.87 \times 10^{18} \text{ cm}^{-3}$)²⁹ and CuGaTe_2 ($1.1 \times 10^{18} \text{ cm}^{-3}$)¹ but is comparable to that of AgGaTe_2 ($1.13 \times 10^{16} \text{ cm}^{-3}$)⁵. However, the mobility μ value ($87.0 \text{ cm}^2/\text{Vs}$) of AgGaTe_2 at RT is much higher than that of AgInTe_2 , which implies that AgInTe_2 has a much larger electrical resistivity than AgGaTe_2 ($\sim 1.0 \times 10^2 \text{ m}\Omega \text{ cm}$ at RT)⁵, even though the bandgap of AgInTe_2 ($E_g = 1.04 \text{ eV}$)¹² is less than that of AgGaTe_2 ($E_g = \sim 1.2 \text{ eV}$)³⁰.

The thermoelectric performance of $\text{Ag}_{1-x}\text{InTe}_2$ before heat treatment as a function of temperature are presented in Fig. 3(a–d), where the Fig. 3a presents the temperature dependence of the Seebeck coefficients (α). All the α values are positive, indicating that the materials exhibit a p-type semiconductor behavior. At first, the α values for most samples increase as the temperature increases up to $\sim 620 \text{ K}$, and then they rapidly decrease until at 660 K . Above $\sim 660 \text{ K}$ the α values increase again as the temperature increases. Such a zigzag-shaped relation is likely attributed to the phase transition in the materials, which will be discussed below.

Figure 3b presents the electrical conductivities (σ) as a function of temperature, where the σ values increase with the increase of the temperature, but they slightly decrease as the x value increases. At 725 K , the σ value of the sample at $x=0.15$ reaches the highest ($8.56 \times 10^2 \Omega^{-1} \text{ m}^{-1}$), and then it decreases to $5.15 \times 10^2 \Omega^{-1} \text{ m}^{-1}$ at 814 K .

The lattice thermal conductivities (κ_L) are displayed in Fig. 3c. Generally, they reduce as the temperature increases. More specifically, the κ_L values reduce rapidly when the temperature is higher than $\sim 620 \text{ K}$; however, above 660 K they reduce relatively slowly. The abrupt changes in κ_L are similar to those observed in the Seebeck coefficients, confirming the phase transitions at these two temperatures. Further, the lattice part (κ_L) at $\sim 814 \text{ K}$ is $0.1 \text{ WK}^{-1} \text{ m}^{-1}$ for the sample at $x=0.15$, about a half that at $x=0$. Generally, the κ_L values are rather low compared to the reported counterparts CuInTe_2 ,^{2,9,10,31,32} and CuGaTe_2 ,^{33–35} but are comparable to those in AgGaTe_2 .⁴ The total κ values of the samples, which are presented in Fig. 3c as an inset, bear resemblance to the lattice parts (κ_L), suggesting that the phonon transport dominates the heat conduction.

Combined with the above three parameters (α , σ , κ), we obtain the ZT values shown in Fig. 3d. The ZT values, which are less than 0.2 for all the samples below 700 K , rapidly increase with the increase of the temperature. At 814 K the ZT value reaches 0.55 for the sample at $x=0.15$. This value is about 1.8 times that of the pristine AgInTe_2 with no heat treated.

One of the factors that contributes to the enhancement in the ZT value in this work is the higher measuring temperature ($\sim 814 \text{ K}$) than the reported one ($\sim 600 \text{ K}$)^{11,13}, above which the TE performance of the materials are seldom reported in the previous documents, likely due to the thermal instability issue.

In order to gain a deep understanding of the thermal stability of the materials, the DSC analysis of the material $\text{Ag}_{1-x}\text{InTe}_2$ ($x=0.15$) was made in the heating process. The result is shown in Fig. 4a, in which we have observed

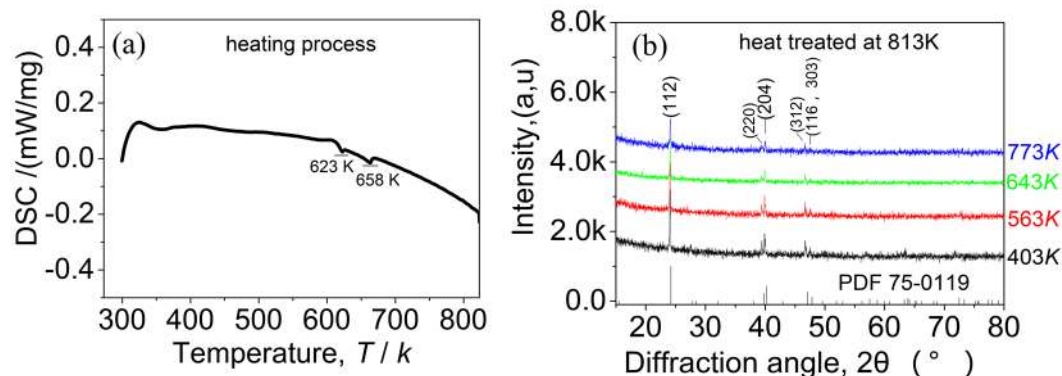


Figure 4. (a) Differential scanning calorimetry (DSC) signal as a function of temperature for the material $\text{Ag}_{0.85}\text{InTe}_2$ with heat treatment, where two exothermic effects at 623 K and 658 K were observed in the heat processing; (b) High temperature diffraction XRD patterns of heat treated material $\text{Ag}_{0.85}\text{InTe}_2$.

two endothermic effects at ~ 623 K and 658 K, corresponding to the phase transitions mentioned above. Although the high temperature XRD patterns (403 K–773 K), shown in Fig. 4b, are insufficient to demonstrate the phase transitions, as all the diffraction peaks can be indexed to the chalcopyrite AgInTe_2 (PDF:75-0119) with no visible movement of the peak positions, we can not rule out the possibility that the materials have undergone order-disorder transitions. These transitions are formed due to the Ag-In antisite occupancy starting in the critical temperatures¹¹, as was observed in the Cu-containing I-III-VI₂ ternary chalcopyrites^{36–38}. At around ~ 620 K, the partial chalcopyrite structure (assumed to be the α phase) is transitioned to sphalerite structure (β phase) followed by the co-existence of the two phase field ($\alpha + \beta$) in the temperature range from 620 K to 655 K. The transition from the α to β phase likely results from the formation of In_{Ag} antisite defect. However, above ~ 655 K, the high energy allows all the α phase to be transformed to the β phase. Alternatively, the β phase returns to the α phase above 655 K due to the dissolution of the antisite defect In_{Ag} . The order-disorder transformation was also observed in the ZnTe-doped CuInTe_2 system³⁹. However, it is very difficult to unravel its nature at the moment, and a detailed investigation and analysis is therefore necessary. Anyhow, what is certain is that the abrupt changes of the Seebeck coefficients at around 620 K and 660 K should be caused by the phase transitions, rather than by the precipitation of the impurity phase Te and/or AgTe_3 since all the samples have similar transitions at these temperatures, including the sample at $x = 0.1$ with no impurity phases precipitated (see Fig. S3b). Although the heat-treated sample at $x = 0.15$ was purified with only trace impurity Te in the matrix, it exhibits the similar temperature dependence of the TE performance to the non-treated samples (see Fig. 3a–d). In addition, the heat-treated sample at $x = 0.15$ gives the highest ZT value of 0.62 at 814 K, more than 2 times that of the pristine AgInTe_2 .

Another contribution to the remarkable improvement in TE performance at high temperatures results from the extremely low lattice part ($\kappa_L = 0.1 \text{ WK}^{-1}\text{m}^{-1}$ for the sample $x = 0.15$), as the highest power factors for the samples, which range from $7.2 \mu\text{W}/\text{cm}^2\text{K}^2$ to $8.3 \mu\text{W}/\text{cm}^2\text{K}^2$ around 814 K, are almost the same (see Fig. S5). The low lattice part (κ_L) is in a good agreement with the glass thermal conductivity $\sim 0.11 \text{ WK}^{-1}\text{m}^{-1}$ estimated by using the Cahill formula^{1,40} below:

$$\kappa_{\min} \sim 1.2 \frac{k_B}{\Omega^{2/3}} \frac{v_l + 2v_s}{3} \quad (1)$$

Here, the k_B , Ω , v_l and v_s are the Boltzmann constant, volume per atom, longitudinal and shear sound velocities. In this estimation, however, the average of the speed of sound (v_m) is used. Therefore, the κ_{\min} of AgInTe_2 ($\sim 0.11 \text{ WK}^{-1}\text{m}^{-1}$) can be easily deduced from the κ_{\min} value ($0.18\text{--}0.23 \text{ WK}^{-1}\text{m}^{-1}$) of AgGaTe_2 ⁷, by using the v_m (1240 m/s) and Debye temperature Θ_D (156 K) of AgInTe_2 and v_m (2402 m/s) and Θ_D (192 K) of AgGaTe_2 ⁷. The ultralow lattice part in $\text{Ag}_{1-x}\text{InTe}_2$ is largely attributed to the enhanced phonon scattering on the point defects due to the increased concentration of the silver vacancy (V_{Ag}).

In order to confirm the dominant effect of the silver vacancy on the unexpected low κ_L , we performed a theoretical calculation of the lattice thermal conductivity based on the Callaway model⁴¹, under the assumption that the Umklapp and point defect scatterings are the main scattering mechanisms. In this case, the ratio ($\kappa_{L,F}/\kappa_{L0}$) of the modeled lattice thermal conductivity of the V_{Ag} -containing samples, $\kappa_{L,F}$ to that of the experimentally determined lattice thermal conductivity without V_{Ag} , κ_{L0} , is shown in Eq. 2,

$$\frac{\kappa_{L,F}}{\kappa_{L0}} = \frac{\tan^{-1}(u)}{u} \quad u^2 = \frac{\pi^2 \Theta_D \Omega}{\hbar V_m^2} \kappa_{L0} \Gamma \quad (2)$$

Here u and Γ are the disorder scaling parameter and the disorder scattering parameter. The v_m , and \hbar are the mean sound velocity and Planck constant. We use the factor Γ below (Eq. 3)⁹ to predict the $\kappa_{L,F}$ values for the AgInTe_2 -based chalcogenides, and the related parameters are presented in Table 1.

Symbol	Representation
Θ_D	Debye temperature, 156 K (ref. ¹³)
ν_m	Average sound velocity, 1240 ms ⁻¹ (ref. ¹³)
h	Planck constant
Ω	Average volume per atom
ϵ_0	9.2 (ref. ¹³)
ϵ	15.64 (ref. ¹³)

Table 1. Parameters used for estimating the lattice thermal conductivity (κ_L) at $x = 0.15$ using Callaway model.

Tem. (K)	$x = 0$ $V_{Ag} = 0$		$x = 0.1, V_{Ag} = 0.05$		$x = 0.15, V_{Ag} = 0.075$		$x = 0.2, V_{Ag} = 0.1$	
	$\kappa_{L,exp.}$	$\kappa_{L,F}$	Γ	U	$\kappa_{L,exp.}$	$\kappa_{L,F}$	Γ	U
328	0.93	0.99	0.99	0.79	0.88	0.71	0.84	
374	0.84	0.89	0.89	0.66	0.80	0.64	0.76	
499	0.65	0.71	0.69	0.60	0.62	0.51	0.59	
567	0.59	0.61	0.63	0.53	0.56	0.46	0.53	
626	0.45	0.51	0.48	0.47	0.43	0.42	0.41	
725	0.22	0.22	0.23	0.31	0.31	0.27	0.27	
764	0.19	0.16	0.20	0.17	0.18	0.17	0.17	
814	0.17	0.14	0.18	0.10	0.16	0.12	0.16	

Table 2. Calculated lattice thermal conductivities ($\kappa_{L,cal.}$) of the sample at $x = 0-0.2$ from the experimental $\kappa_{L,exp.}$ at $x = 0$.

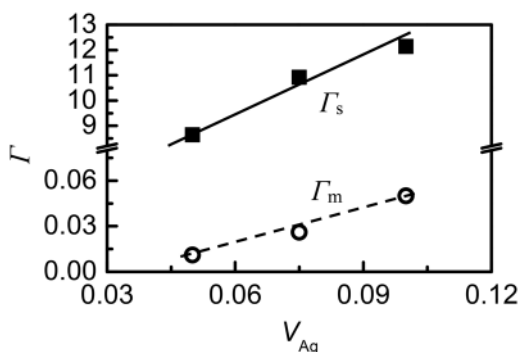


Figure 5. The mass fluctuations Γ_m and strain field fluctuations Γ_s for three samples at $x = 0.1, 0.15$ and 0.2 as a function of silver vacancy V_{Ag} ($V_{Ag} = x_i/2$).

$$\Gamma = x_i(1 - x_i) \left[\left(\frac{\Delta M_i}{M} \right)^2 + \epsilon \left(\frac{\Delta \delta_i}{x_i \delta} \right)^2 \right] \quad (3)$$

In Eq. 3, the parameters x_i , $\Delta M_i/M$ and $\Delta \delta_i/\delta$ are the molar fraction of Ag, mass difference, and the local change in lattice parameters.

Based on the above calculations, the mass fluctuations Γ_m and strain field fluctuations Γ_s for three samples at $x = 0.1, 0.15$ and 0.2 are displayed in Fig. 5 as a function of silver vacancy ($V_{Ag} = x_i/2$), while the fitted $\kappa_{L,F}$ values, the disorder scaling parameter (u) and the disorder scattering parameter (Γ) consisting of Γ_m and Γ_s are presented in Table 2. It is observed that the strain field fluctuations Γ_s is mainly responsible for the lattice disorder, while the mass fluctuations Γ_m plays a minor role. The fitted $\kappa_{L,F}$ values are roughly in accordance with the experimentally determined κ_L values, except for those at high temperatures, which are about 30–60% higher than the measured ones at 814 K (see Table 2). The origin for the high estimated $\kappa_{L,F}$ values is due to the fact that the extra phonon scattering on the distorted crystal structure is not taken into account. This distortion, which is caused by the different interactions between the bonds Ag-Te and In-Te and represented by the higher anion position parameter u ($u \approx 0.258 > 0.25$, in Fig. 1b,c), has a profound impact on the lattice part κ_L ^{42,43}. However, the phonon scattering on the increased phase boundaries due to the presence of the impurity phases (AgTe₃ and Te) should play a minor role, as it acts only at low to middle temperatures.

Having figured out the phonon scattering mechanism, we thus propose that the low lattice part κ_L at high temperatures mainly results from the Umklapp scattering, extra point defect and crystal structure distortion. However, the phonon scattering by the carriers weakens as the carrier concentration (n_H) reduces, which neutralizes the increased phonon scattering to some extent.

Conclusions

In this work we prepared the $\text{Ag}_{1-x}\text{InTe}_2$ ($x = 0-0.2$) with substoichiometric amounts of Ag and examined their thermoelectric performance. The analyses reveal that the main phase AgInTe_2 undergoes phase transitions at ~ 620 K and ~ 655 K, even though there are minor impurity phases (element Te and/or AgTe_3) precipitated. Upon the increasing of silver vacancy (V_{Ag}) concentration, an ultralow lattice thermal conductivity ($\kappa_L = 0.1 \text{ Wm}^{-1}\text{K}^{-1}$) at $x = 0.15$ was attained, and a more than 2-fold enhancement in ZT value achieved at 814 K compared to the pristine AgInTe_2 . Besides, the origin of the ultralow lattice part κ_L is decoupled and elucidated using the Callaway model, proving that the silver vacancy concentration engineering is still an effective way to manipulate the thermoelectric performance of AgInTe_2 .

Data availability

The datasets generated during and/or analyzed during the current study are available from the corresponding author on reasonable request.

Received: 31 July 2019; Accepted: 28 November 2019;

Published online: 11 December 2019

References

- Plirdpring, T. *et al.* Chalcopyrite CuGaTe_2 : A high-efficiency bulk thermoelectric material. *Adv. Mater.* **24**, 3622–3626 (2012).
- Luo, Y. *et al.* Progressive regulation of electrical and thermal transport properties to high-performance CuInTe_2 thermoelectric materials. *Adv. Energy Mater.* **6**, 1600007 (2016).
- Qiu, P. *et al.* Intrinsically high thermoelectric performance in AgInSe_2 n-Type diamond-like compounds. *Adv. Sci.* **4**, 1700727 (2017).
- Wu, W. *et al.* Doping and temperature dependence of thermoelectric properties of AgGaTe_2 : First principles investigations. *Chem. Phys. Lett.* **537**, 62–64 (2012).
- Yusufu, A. *et al.* Thermoelectric properties of $\text{Ag}_{1-x}\text{GaTe}_2$ with chalcopyrite structure. *Appl. Phys. Lett.* **99**, 061902 (2011).
- Miglio, A. *et al.* Local bonding influence on the band edge and band gap formation in quaternary chalcopyrites. *Adv. Sci.* **4**, 1700080 (2017).
- Su, X. *et al.* High thermoelectric performance in the wide band-gap $\text{AgGa}_{1-x}\text{Te}_2$ compounds: directional negative thermal expansion and intrinsically low thermal conductivity. *Adv. Funct. Mater.* **29**, 1806534 (2018).
- Shen, J. *et al.* Vacancy scattering for enhancing the thermoelectric performance of CuGaTe_2 solid solutions. *J. Mater. Chem. A* **4**, 15464 (2016).
- Xia, Z. *et al.* Effect of the Cu vacancy on the thermoelectric performance of p-type $\text{Cu}_{1-x}\text{InTe}_2$ compounds. *Ceram. Int.* **43**, 16276–16282 (2017).
- Liu, R. *et al.* Thermoelectric performance of $\text{Cu}_{1-x}\text{Ag}_x\text{InTe}_2$ diamond-like materials with a pseudocubic crystal structure. *Inorg. Chem. Front.* **3**, 1167–1177 (2016).
- Bellabarba, C. Electrical properties of AgInTe_2 . *Mater. Lett.* **36**, 299–302 (1998).
- Fujii, Y. *et al.* Relationship between electrical properties and electronic structure of the thermoelectric Ag-In-Te system with chalcopyrite structure and its related defect-containing structure. *Scripta Mater.* **162**, 272–276 (2019).
- Aikebaiera, Y. *et al.* High-temperature thermoelectric properties of non-stoichiometric $\text{Ag}_{1-x}\text{InTe}_2$ with chalcopyrite structure. *Mater. Sci. Eng. B* **177**, 999–1002 (2012).
- Bellabarba, C. *et al.* Thermal conductivity of AgInTe_2 . *Phys. Stat. Sol. (a)* **66**, K105–K108 (1981).
- Charoenphakdee, A. *et al.* Thermal conductivity of the ternary compounds: AgMTe_2 and AgM_2Te_8 ($M = \text{Ga}$ or In). *Mater. Trans.* **50**, 1603–1606 (2009).
- Fernández, B. *et al.* Sound velocities and elastic moduli in CuInTe_2 and CuInSe_2 . *Phys. Stat. Sol. (a)* **122**, 235–242 (1990).
- Ying, P. *et al.* Hierarchical chemical bonds contributing to the intrinsically low thermal conductivity in α - MgAgSb thermoelectric materials. *Adv. Funct. Mater.* **27**, 1604145 (2017).
- Neumann, H. Vacancy formation enthalpies in $\text{A}^{\text{I}}\text{B}^{\text{II}}\text{C}^{\text{VI}}$ chalcopyrite semiconductors. *Crystal Res. Technol.* **18**, 901–906 (1983).
- Schröder, T. *et al.* TAGS-related indium compounds and their thermoelectric properties—the solid solution series $(\text{GeTe})_x\text{AgIn}_y\text{Sb}_{1-y}\text{Te}_2$ ($x = 1-12$; $y = 0.5$ and 1). *J. Mater. Chem. A* **2**, 6384–6395 (2014).
- Kopytov, A. V. *et al.* Thermodynamic and elastic properties of AgInSe_2 and AgInTe_2 . *Phys. Solid State* **52**, 1359–1361 (2010).
- Zhong, Y. Elastic, vibration and thermodynamic properties of $\text{Cu}_{1-x}\text{Ag}_x\text{InTe}_2$ ($x = 0, 0.25, 0.5, 0.75$ and 1) chalcopyrite compounds via first principles. *Semicond. Sci. Technol.* **33**, 065014 (2018).
- Kim, H. *et al.* Characterization of Lorenz number with Seebeck coefficient measurement. *APL Mater.* **3**, 041506 (2015).
- Kasiviswanathan, S. *et al.* Preparation and characterization of the pseudobinary system $\text{Cu}_{1-x}\text{Ag}_x\text{InTe}_2$. *J. Mater. Sci. Lett.* **5**, 912–914 (1986).
- Plirdpring, T. *et al.* Effect of the amount of vacancies on the thermoelectric properties of Cu-Ga-Te ternary compounds. *Mater. Trans.* **53**, 1212–1215 (2012).
- Guedez, E. *et al.* Crystal structure, electrical, and optical properties of $\text{Cu}_3\text{In}_7\text{Te}_{12}$ ordered defect semiconducting compound. *Phys. Status Solidi (b)* **254**, 1700087 (2017).
- Ye, Z. *et al.* The effect of structural vacancies on the thermoelectric properties of $(\text{Cu}_2\text{Te})_{1-x}(\text{Ga}_2\text{Te}_3)_x$. *J. Solid State Chem.* **201**, 262–269 (2013).
- Cui, J. *et al.* Significantly enhanced thermoelectric performance of γ - In_2Se_3 through lithiation via chemical diffusion. *Chem. Mater.* **29**, 7467–7474 (2017).
- Cui, J. *et al.* Engineering band structure via the site preference of Pb^{2+} in the In^+ site for enhanced thermoelectric performance of In_6Se_7 . *ACS Appl. Mater. Interfaces* **8**, 23175–23180 (2016).
- Liu, R. *et al.* Ternary compound CuInTe_2 : a promising thermoelectric material with diamond-like structure. *Chem. Commun.* **48**, 3818–3820 (2012).
- Ohmer, M. *et al.* Infrared properties of AgGaTe_2 , a nonlinear optical chalcopyrite semiconductor. *J. Appl. Phys.* **86**, 94–99 (1999).
- Chen, H. *et al.* Thermoelectric properties of CuInTe_2 /graphene composites. *CrystEngComm* **15**, 6648–6651 (2013).
- Kosuga, A. *et al.* Room-temperature pressure-induced nanostructural CuInTe_2 thermoelectric material with low thermal conductivity. *Inorg. Chem.* **53**, 6844–6849 (2014).

33. Carr, W. *et al.* Influence of doping and solid solution formation on the thermoelectric properties of chalcopyrite semiconductors. *J. Alloy. Compd.* **630**, 277–281 (2015).
34. Zhang, J. *et al.* Enhanced thermoelectric properties of Ag-doped compounds $\text{CuAg}_x\text{Ga}_{1-x}\text{Te}_2$ ($0 \leq x \leq 0.05$). *J. Alloy. Compd.* **586**, 285–288 (2014).
35. Shen, J. *et al.* Substitutional defects enhancing thermoelectric CuGaTe_2 . *J. Mater. Chem. A*. **5**, 5314–5320 (2017).
36. Zunger, A. Order-disorder transformation in ternary tetrahedral semiconductors. *Appl. Phys. Lett.* **50**, 164–166 (1987).
37. Schorr, S. *et al.* Some are different from others: high temperature structural phase transitions in ternary chalcopyrites. *Phys. Stat. Sol. (c)* **3**, 2610–2613 (2006).
38. Rinón, C. On the order-disorder phase transition in ternary compounds. *Solid State Commun.* **64**, 663–665 (1987).
39. Roussak, L. *et al.* Phase relationships in the pseudo-binary $2(\text{ZnTe})\text{-CuInTe}_2$ system. *J. Solid State Chem.* **178**, 3476–3484 (2005).
40. Cahill, D. G. *et al.* Lower limit to the thermal conductivity of disordered crystals. *Phys. Rev. B*. **46**, 6131–6140 (1992).
41. Callaway, J. *et al.* Effect of point imperfections on lattice thermal conductivity. *Phys. Rev.* **120**, 1149 (1960).
42. Heinrich, C. *et al.* Effect of isovalent substitution on the thermoelectric properties of the $\text{Cu}_2\text{ZnGeSe}_{4-x}\text{S}_x$ series of solid solutions. *J. Am. Chem. Soc.* **136**, 442–448 (2014).
43. Zhao, L. *et al.* Regulation of the crystal structure leading to the bandgap widening and phonon scattering increasing in $\text{Cu}_3\text{SnS}_4\text{-Cu}_3\text{SbSe}_3$ chalcogenides. *Adv. Electron. Mater.* **5**(1900485), 1–7 (2019).

Acknowledgements

This work is supported by the National Natural Science Foundation of China (51671109, 51171084).

Author contributions

Jiaolin Cui designed the study and wrote the manuscript; Yaqiong Zhong and Yong Luo prepared materials & samples and performed experiments & analyses on thermoelectric transport properties; Yaqiong Zhong was also responsible for the preparation of the images/drawings/photographs; Xie Li was responsible for the structural analyses and observations of the microstructures.

Competing interests

The authors declare no competing interests.

Additional information

Supplementary information is available for this paper at <https://doi.org/10.1038/s41598-019-55458-3>.

Correspondence and requests for materials should be addressed to Y.L. or J.C.

Reprints and permissions information is available at www.nature.com/reprints.

Publisher's note Springer Nature remains neutral with regard to jurisdictional claims in published maps and institutional affiliations.



Open Access This article is licensed under a Creative Commons Attribution 4.0 International License, which permits use, sharing, adaptation, distribution and reproduction in any medium or format, as long as you give appropriate credit to the original author(s) and the source, provide a link to the Creative Commons license, and indicate if changes were made. The images or other third party material in this article are included in the article's Creative Commons license, unless indicated otherwise in a credit line to the material. If material is not included in the article's Creative Commons license and your intended use is not permitted by statutory regulation or exceeds the permitted use, you will need to obtain permission directly from the copyright holder. To view a copy of this license, visit <http://creativecommons.org/licenses/by/4.0/>.

© The Author(s) 2019